INTERNATIONAL JOURNAL FOR NUMERICAL METHODS IN ENGINEERING
Int. J. Numer. Meth. Engng 2002; **53**:1801–1829 (DOI: 10.1002/nme.361)

Time-discretized variational formulation of non-smooth frictional contact

A. Pandolfi[1], C. Kane[2], J. E. Marsden[2] and M. Ortiz[2,*,†]

[1] *Dipartimento di Ingegneria Strutturale, Politecnico di Milano, 20133 Milano, Italy*
[2] *Control and Dynamical Systems, Graduate Aeronautical Laboratories, California Institute of Technology, Pasadena, CA 91125, U.S.A.*

SUMMARY

The present work extends the non-smooth contact class of algorithms introduced by Kane *et al.* to the case of friction. The formulation specifically addresses contact geometries, e.g. involving multiple collisions between tightly packed non-smooth bodies, for which neither normals nor gap functions can be properly defined. A key aspect of the approach is that the incremental displacements follow from a *minimum* principle. The objective function comprises terms which account for inertia, strain energy, contact, friction and external forcing. The Euler–Lagrange equations corresponding to this extended variational principle are shown to be consistent with the equations of motion of solids in frictional contact. In addition to its value as a basis for formulating numerical algorithms, the variational framework offers theoretical advantages as regards the selection of trajectories in cases of non-uniqueness. We present numerical and analytical examples which demonstrate the good momentum and energy conservation characteristics of the numerical algorithms, as well as the ability of the approach to account for stick and slip conditions. Copyright © 2001 John Wiley & Sons, Ltd.

KEY WORDS: non-smooth frictional contact; incremental variational formulation; time-stepping algorithms; closest point projection; non-smooth analysis

1. INTRODUCTION

The present work aims to extend the non-smooth contact algorithm of Kane *et al.* [1] to the case of friction. The approach specifically addresses multibody non-smooth geometries, for which neither normals nor gap functions can be defined. Examples of such situations include granular flows and brittle solids undergoing fragmentation. For instance, ballistic impact of

*Correspondence to: M. Ortiz, Graduate Aeronautical Laboratories, Firestone Flight Sciences Laboratory, California Institute of Technology, Pasadena, CA 91125, U.S.A.
†E-mail: ortiz@aero.caltech.edu

Contract/grant sponsor: AFOSR, partially; contract/grant number: F49620-96-1-0471
Contract/grant sponsor: DoE, partially
Contract/grant sponsor: Army Research Office; contract/grant number: DAAH04-96-1-0056

Received 4 September 2000
Revised 18 January 2001

brittle targets often results in the formation of large numbers of fragments which undergo complex collision sequences before eventually scattering [2, 3]. During the early stages of fragmentation, the corners of many angular fragments may come together at a point, which precludes the definition of a gap function as a means of detecting—and constraining—their interpenetration. Fragments are tightly packed initially, leading to contact situations which involve potential collisions between a large number of bodies. In addition, the non-smooth character of the fragments has the consequence that normals are not defined in the usual sense in the contact region. We refer to contact processes such as those just described, involving the simultaneous interaction between many angular bodies, as *non-smooth contact*.

Most contact/friction algorithms proposed to date envision two smooth bodies in contact and use a gap function to constrain or penalize interpenetration (see, e.g. References [4–27]). The approaches in these papers can be viewed as a regularization of the well-known Signorini condition, which relates the contact forces to a convenient measure of the distance between the contacting bodies. Though otherwise effective and widely used, most of these methods do not appear to be readily applicable to the analysis of non-smooth contact.

Frictional contact is a complex phenomenon which has been addressed in an extensive body of literature [28–57]. In contact problems, frictional effects are generally accounted for by the introduction of a friction law which relates the sliding velocity to the contact forces. The tangential component of the contact tractions, or frictional traction, can be exerted without sliding, i.e. under *stick* conditions, until a certain threshold is overcome to allow sliding. In Coulomb's law, the threshold is proportional to the magnitude of the normal pressure; when sliding occurs, the frictional tractions always oppose the sliding velocity and are, therefore, dissipative.

Frictionless non-smooth contact algorithms have been recently introduced and discussed by Kane *et al.* [1]. That work is based on *non-smooth analysis* (see Reference [58]) which provides a general characterization of the non-smooth contact forces and the analytical tools required for treating time-discretized approximations. Non-smooth calculus has been used before by other authors in contact problems (such as References [59, 60]), but the goals and specific techniques are different. The impenetrability constraint is enforced by detecting intersections between pairs of boundary triangles. This approach does not require any assumption of smoothness of the boundary and enables the analysis of contact between sharp features such as edges and vertices. An important observation is that non-smooth algorithms bear a resemblance to those which are suggested by the mathematical theory of plasticity (see, e.g. References [60–64]), especially as regards the use of *closest-point projections*, an analogy which has been noted by Laursen and Govindjee [65]. However, it should be noted that the admissible sets which arise in contact problems are generally *non-convex*, which precludes the direct application of convex analysis.

The primary goal of the present paper is to demonstrate that the non-smooth contact approach of Kane *et al.* [1] and its variational structure do indeed extend in a satisfactory way to the case of frictional contact. Our treatment of friction fits within the general variational framework for dynamic and dissipative problems developed by Ortiz *et al.* [66, 64, 67]. This approach relies on time-discretization and leads to the formulation of *minimum* principles characterizing the solutions of the incremental problem. The function to be minimized contains both conservative and dissipative terms, and may be regarded as an incremental potential energy. For the class of problems under consideration here, the incremental potential energy comprises terms which account for inertia, strain energy, contact, friction and

external forcing. The frictional term is incremental and dissipative, as befits friction. Minimization of the incremental potential energy delivers a solution consistent with the equations of motion of solids in frictional contact. In particular, the formulation is capable of accounting for stick–slip conditions.

The organization of the paper is as follows. In Section 2, we introduce relevant concepts on non-smooth analysis and non-smooth contact. In Section 3, the case of frictionless non-smooth contact is treated by way of introduction. In Sections 4, we illustrate the advantages of the variational approach to contact in problems where multiple trajectories are possible. In Sections 5 and 6 the non-smooth contact formulation is generalized to account for friction. In Section 7 simple one- and two-dimensional examples are developed in detail to demonstrate the properties of the algorithm. Finally, in Section 8 the good performance of the algorithm is demonstrated with the aid of selected examples.

2. GENERAL FRAMEWORK

In this section we review selected aspects of the mechanics of collisions that will be helpful in subsequent discussions, with particular emphasis on the variational formulation of contact problems for deformable bodies. We specifically focus on the finite-element solution of contact problems, and thus we confine our discussion of non-smooth analysis to the finite-dimensional case.

We shall be concerned with the motions of a deformable body occupying a domain $B_0 \subset \mathbb{R}^d$ in its reference configuration. The deformations of interest are described by deformation mappings $\boldsymbol{\varphi} : B_0 \times [0, T] \to \mathbb{R}^d$ subordinate to a finite element discretization of B_0. Here $[0, T]$ is the time duration of the motion. For a fixed $t \in [0, T]$, the deformation mappings $\boldsymbol{\varphi}(\cdot, t)$ define a finite-dimensional space X. By a slight abuse of notation, we shall variously take $\boldsymbol{\varphi}$ to denote the discretized deformation field or the array of nodal coordinates in the deformed configuration. For simplicity, we shall assume the solid to be elastic. Extensions to inelasticity may be effected simply by the introduction of appropriately defined incremental strain-energy densities [66, 64, 67].

In the absence of contact constraints, the action functional for the solid is of the form

$$I[\boldsymbol{\varphi}] = \int_0^T \left[\frac{1}{2} \dot{\boldsymbol{\varphi}}^{\mathrm{T}} \mathbf{M} \dot{\boldsymbol{\varphi}} - \phi(\boldsymbol{\varphi}) + \mathbf{f}^{\mathrm{ext}} \cdot \boldsymbol{\varphi} \right] \mathrm{d}t \tag{1}$$

where $\mathbf{M}$ is the mass matrix of the solid, $\phi(\boldsymbol{\varphi})$ denotes its strain energy and $\mathbf{f}^{\mathrm{ext}}(t)$ are the externally applied forces. The equations of motion of the spatially discretized solid follow by requiring that $I[\boldsymbol{\varphi}]$ be stationary, with the result

$$\mathbf{M} \ddot{\boldsymbol{\varphi}} + \mathbf{f}^{\mathrm{int}}(\boldsymbol{\varphi}) = \mathbf{f}^{\mathrm{ext}} \tag{2}$$

where

$$\mathbf{f}^{\mathrm{int}} = \nabla \phi(\boldsymbol{\varphi}) \tag{3}$$

are the internal forces. Equation (2), in conjunction with initial conditions of the form

$$[\boldsymbol{\varphi}]_{t=0} = \boldsymbol{\varphi}_{h0} \tag{4}$$

$$[\dot{\boldsymbol{\varphi}}]_{t=0} = \dot{\boldsymbol{\varphi}}_{h0} \tag{5}$$

defines an initial value problem to be solved for $\boldsymbol{\varphi}$.

We extend the above formulation to non-smooth contact problems with the aid of non-smooth analysis. A complete account on non-smooth analysis may be found in the monograph [58]. A brief review of concepts relevant to the present context is given in Reference [1]. We begin by considering the restrictions imposed on the motion of the bodies by the impenetrability constraint. The notion of an *admissible set* of deformations will play a central role to that effect. The admissible set C is simply the set of the deformation mappings which are globally one-to-one in X. Physically, $\boldsymbol{\varphi} \in C$ if and only if the deformation mapping $\boldsymbol{\varphi}$ does not entail separation or interpenetration of matter.

As is commonly done in the so-called *barrier* methods, the interpenetration constraint may be accounted for by adding the indicator function $I_C(\boldsymbol{\varphi})$ of the admissible set C to the energy of the solid. The indicator of a set C is the extended-valued function

$$I_C(\mathbf{x}) = \begin{cases} 0 & \text{if } \mathbf{x} \in C \\ \infty & \text{otherwise} \end{cases} \tag{6}$$

Introducing I_C, the action functional becomes

$$I(\boldsymbol{\varphi}) = \int_0^T \left[\frac{1}{2} \dot{\boldsymbol{\varphi}}^{\mathrm{T}} \mathbf{M} \dot{\boldsymbol{\varphi}} - \phi(\boldsymbol{\varphi}) - I_C(\boldsymbol{\varphi}) + \mathbf{f}^{\mathrm{ext}} \cdot \boldsymbol{\varphi} \right] \mathrm{d}t \tag{7}$$

Evidently, from definition (6) of the indicator function of a set, it follows that the additional term in the energy effectively bars the trajectories from exiting the admissible set C, i.e. from violating the interpenetration constraint.

The problem is now to determine the absolutely continuous trajectories $\boldsymbol{\varphi}(t)$ which render the action stationary (cf. Reference [58]). From the stationarity principle, it follows that the trajectories are weak solutions of the equation

$$\mathbf{0} \in \mathbf{M} \ddot{\boldsymbol{\varphi}} + \mathbf{f}^{\mathrm{int}}(\boldsymbol{\varphi}) + \partial I_C(\boldsymbol{\varphi}) - \mathbf{f}^{\mathrm{ext}} \tag{8}$$

where

$$\mathbf{f}^{\mathrm{int}}(\boldsymbol{\varphi}) = \partial \phi(\boldsymbol{\varphi}) \tag{9}$$

are the internal forces and ∂I_C is the generalized gradient of the indicator function [58]. Equation (8), in conjunction with initial conditions (4) and (5), defines an initial value problem to be solved for $\boldsymbol{\varphi}$. In Equation (8), the term $\partial I_C(\boldsymbol{\varphi})$ represents the contact forces over the configuration $\boldsymbol{\varphi}$, so that

$$\mathbf{f}^{\mathrm{con}}(\boldsymbol{\varphi}) = \partial I_C(\boldsymbol{\varphi}) \tag{10}$$

The generalized gradient reduces to the ordinary derivative at points where the function is continuously differentiable. It also reduces to the subdifferential in the case of convex functions. A precise definition of the generalized gradient of a Lipschitz function and related properties may be found in References [58, 1]. Physically, the set $\partial I_C(\boldsymbol{\varphi})$ consists of all the contact force fields corresponding to a configuration $\boldsymbol{\varphi}$. Thus, if the surfaces in contact are smooth, $\partial I_C(\boldsymbol{\varphi})$ consists of all normal and compressive force fields over the area of contact. In the non-smooth case, the set of contact reactions may include cones centered at the corners of the surfaces in contact.

Kane *et al.* [1] have provided computationally efficient characterizations of the admissible set C for polyhedra, e.g. such as result from a triangulation of the domain of the solid by simplices, in the form of a collection of algebraic inequality constraints on the nodal displacements of the general form

$$g_\alpha(\boldsymbol{\varphi}) \geqslant 0, \quad \alpha = 1, \ldots, N \tag{11}$$

where N is the total number of possible contact constraints. Each constraint enforces the absence of intersection between a given pair of boundary simplices, i.e. segments and triangles in two and three dimensions, respectively. Thus, N is the total number of pairs of distinct simplices in the triangulation of the boundary. The precise set of algebraic constraints employed in the calculations reported here is described in Appendix A.

In terms of the contact constraints (11), the admissible set follows as

$$C = \{\boldsymbol{\varphi} : B_{0h} \times [0, T] \to \mathbb{R}^d \mid g_\alpha(\boldsymbol{\varphi}) \geqslant 0, \ \alpha = 1, \ldots, N\} \tag{12}$$

where B_{0h} denotes the discretized body. Simple examples of admissible sets for systems consisting of a 'particle in a box' have been given by Kane *et al.* [1]. These examples illustrate the fact that the admissible set C is generally non-convex. The system of normal contact forces corresponding to constraint α may be written in the form

$$\mathbf{N}_\alpha = \lambda_\alpha \nabla g_\alpha(\boldsymbol{\varphi}_\alpha) \tag{13}$$

where λ_α is a scalar multiplier which is subject to unilateral constraints and $\boldsymbol{\varphi}_\alpha$ are the local nodal position vector fields corresponding to each one of the contact constraints. Thus, $\boldsymbol{\varphi}_\alpha$ is the collection of position vectors of the nodes attached to the pair of simplices involved in constraint α. The global contact system (10) is obtained by the assembly of all the local normal force systems $\{\mathbf{N}_\alpha, \ \alpha = 1, \ldots, N\}$ in the usual sense of finite elements. We denote this assembly operation symbolically as

$$\mathbf{f}^{\text{con}} = \mathscr{A}(\{\mathbf{N}_\alpha, \ \alpha = 1, \ldots, N\}) \tag{14}$$

It follows from the invariance properties of C that I_C, and by extension the action I, is itself invariant under the action of translations and rotations (assuming that there are no displacement boundary conditions). It follows from Noether's theorem (see, e.g. Reference [68]) that the solutions of (8) conserve linear and angular momentum. Global energy conservation follows likewise from the time independence or autonomous character of the Lagrangian. Additionally, since any admissible solution must necessarily be such that $I_C(\boldsymbol{\varphi}(t)) = 0$, which corresponds to the fact that the contact area does not store or dissipate energy, it follows that the volume energy is also conserved.

3. TIME-DISCRETIZATION: FRICTIONLESS CONTACT

In addition to its traditional role in the formulation of time-stepping algorithms, here time-discretization furnishes the key device enabling the variational formulation of dynamical problems and frictional dissipation in terms of a *minimum*—as opposed to merely a stationary-principle.

Henceforth, we envision an incremental solution procedure whereby $\boldsymbol{\varphi}$ is approximated at discrete times $t_n = n\triangle t$. We begin by specializing (8) to time t_{n+1}, with the result

$$\mathbf{0} \in \mathbf{M}\ddot{\boldsymbol{\varphi}}_{n+1} + \mathbf{f}^{\text{int}}(\boldsymbol{\varphi}_{n+1}) + \mathbf{f}^{\text{con}}(\boldsymbol{\varphi}_{n+1}) - \mathbf{f}^{\text{ext}}_{n+1} \tag{15}$$

where internal and contact forces are given by

$$\mathbf{f}^{\text{int}}(\boldsymbol{\varphi}_{n+1}) = \partial\phi(\boldsymbol{\varphi}_{n+1}), \quad \mathbf{f}^{\text{con}}(\boldsymbol{\varphi}_{n+1}) = \partial I_C(\boldsymbol{\varphi}_{n+1}) \tag{16}$$

As in the case of plasticity (see, e.g. References [61–63]), the robustness of the algorithm requires a fully *implicit* treatment of the contact force system $\partial I_C(\boldsymbol{\varphi}_{n+1})$. By contrast, the remainder of the terms in (15) may be treated either *implicitly* or *explicitly*. In view of this distinction, we split the accelerations into terms due to the internal forces

$$\ddot{\boldsymbol{\varphi}}^{\text{int}}_{n+1} = \mathbf{M}^{-1}[\mathbf{f}^{\text{ext}} - \mathbf{f}^{\text{int}}(\boldsymbol{\varphi}_{n+1})] \tag{17}$$

and the accelerations due to contact forces

$$\ddot{\boldsymbol{\varphi}}^{\text{con}}_{n+1} = -\mathbf{M}^{-1}\mathbf{f}^{\text{con}}(\boldsymbol{\varphi}_{n+1}) \tag{18}$$

A general class of *implicit/explicit* algorithms, in the style of the Newmark family of algorithms [69, 70], is obtained by setting

$$\boldsymbol{\varphi}_{n+1} = \boldsymbol{\varphi}_n + \triangle t\dot{\boldsymbol{\varphi}}_n + \triangle t^2[(1/2-\beta)\ddot{\boldsymbol{\varphi}}^{\text{int}}_n + \beta\ddot{\boldsymbol{\varphi}}^{\text{int}}_{n+1}] + (\triangle t^2/2)\ddot{\boldsymbol{\varphi}}^{\text{con}}_{n+1} \tag{19}$$

$$\dot{\boldsymbol{\varphi}}_{n+1} = \dot{\boldsymbol{\varphi}}_n + \triangle t[(1-\gamma)\ddot{\boldsymbol{\varphi}}^{\text{int}}_n + \gamma\ddot{\boldsymbol{\varphi}}^{\text{int}}_{n+1}] + \triangle t\ddot{\boldsymbol{\varphi}}^{\text{con}}_{n+1} \tag{20}$$

The explicit member of the algorithm, i.e. that which is explicit in the internal forces and implicit in the contact forces, corresponds to the choice $\beta = 0$. We shall refer to the remaining members as implicit/implicit.

The above relations may be simplified by introducing the predictor

$$\boldsymbol{\varphi}^{\text{pre}}_{n+1} = \boldsymbol{\varphi}_n + \triangle t\dot{\boldsymbol{\varphi}}_n + (\tfrac{1}{2}-\beta)\triangle t^2\ddot{\boldsymbol{\varphi}}^{\text{int}}_n \tag{21}$$

whereupon (19) becomes

$$\boldsymbol{\varphi}_{n+1} = \boldsymbol{\varphi}^{\text{pre}}_{n+1} + \beta\triangle t^2\ddot{\boldsymbol{\varphi}}^{\text{int}}_{n+1} + \frac{\triangle t^2}{2}\ddot{\boldsymbol{\varphi}}^{\text{con}}_{n+1} \tag{22}$$

Combining the preceding relations, Equation (15) may be recast in the form

$$\mathbf{0} \in \frac{2}{\triangle t^2}\mathbf{M}(\boldsymbol{\varphi}_{n+1} - \boldsymbol{\varphi}^{\text{pre}}_{n+1}) + 2\beta[\mathbf{f}^{\text{int}}(\boldsymbol{\varphi}_{n+1}) - \mathbf{f}^{\text{ext}}_{n+1}] + \mathbf{f}^{\text{con}}(\boldsymbol{\varphi}_{n+1}) \tag{23}$$

which defines a system of non-linear algebraic equations to be solved for $\boldsymbol{\varphi}_{n+1}$. Once $\boldsymbol{\varphi}_{n+1}$ is computed, the internal accelerations $\ddot{\boldsymbol{\varphi}}^{\text{int}}_{n+1}$follow from (17) and the contact accelerations from (22), with the result

$$\ddot{\boldsymbol{\varphi}}^{\text{con}}_{n+1} = \frac{2}{\triangle t^2}(\boldsymbol{\varphi}_{n+1} - \boldsymbol{\varphi}^{\text{pre}}_{n+1}) - 2\beta\ddot{\boldsymbol{\varphi}}^{\text{int}}_{n+1} \tag{24}$$

Finally, the velocities are computed from (20), which completes an application of the algorithm.

The crux of the algorithm just described consists of the determination of $\boldsymbol{\varphi}_{n+1}$ from (23). A far-reaching realization is that (23) may be expressed in the form

$$\mathbf{0} \in \partial(f(\boldsymbol{\varphi}_{n+1}) + I_C(\boldsymbol{\varphi}_{n+1})) \tag{25}$$

where

$$f(\boldsymbol{\varphi}_{n+1}) = \|\boldsymbol{\varphi}_{n+1} - \boldsymbol{\varphi}^{\text{pre}}_{n+1}\|^2_K + 2\beta[\phi(\boldsymbol{\varphi}_{n+1}) - \mathbf{f}^{\text{ext}}_{n+1} \cdot \boldsymbol{\varphi}_{n+1}] \tag{26}$$

and

$$\|\mathbf{u}\|_K \equiv \frac{1}{\triangle t}\sqrt{\mathbf{u}^{\mathrm{T}}\mathbf{M}\mathbf{u}} \tag{27}$$

may be interpreted as a *kinetic-energy* norm. In the explicit case, with $\beta = 0$ (26) reduces to

$$f(\boldsymbol{\varphi}_{n+1}) = \|\boldsymbol{\varphi}_{n+1} - \boldsymbol{\varphi}^{\text{pre}}_{n+1}\|^2_K \tag{28}$$

The minimizing or *stable* solutions of (25) may now be identified with the solutions of the problem

$$\min_{\boldsymbol{\varphi}_{n+1} \in X} f(\boldsymbol{\varphi}_{n+1}) + I_C(\boldsymbol{\varphi}_{n+1}) \tag{29}$$

which is equivalent to the constrained minimization problem

$$\min_{\boldsymbol{\varphi}_{n+1} \in C} f(\boldsymbol{\varphi}_{n+1}) \tag{30}$$

This is a standard non-linear optimization problem, which may be solved by a variety of methods [71–73]. In the explicit case, the objective function f is quadratic and (30) reduces to a quadratic programming problem. An essential part of the solution of (30) is the determination of the active constraints. This determination in turn has the effect of resolving the precise sequence of the collisions which take place in many-body problems.

It should also be noted that, in the explicit case and provided that the mass matrix is diagonal, the global optimization problem decomposes into uncoupled *local* problems, each involving a small number of degrees of freedom. The local problems are set up by first detecting all intersections between segments (faces), an operation which can be carried out efficiently by recourse to quadtree (octree) searches. The intersecting segments (faces) are then grouped in accordance to their respective adjacencies, with every disjoint group defining a local problem. These local problems may then be solved independently.

The geometrical structure of the algorithms has been investigated by Kane *et al.* [1]. The algorithm is found to have a structure similar to that of the closest-point return mapping

algorithms of plasticity [62, 63], where the closest-point projection here has to be interpreted in energetic terms. The predictor $\boldsymbol{\varphi}_{n+1}^{\mathrm{pre}}$, which is computed without regard to contact, will generally wander off the admissible set C. This violation of the interpenetration constraint is remedied by returning $\boldsymbol{\varphi}_{n+1}^{\mathrm{pre}}$ to the 'closest point' $\boldsymbol{\varphi}_{n+1}$ on C in the sense of the objective function f. In the special case of explicit integration, $\boldsymbol{\varphi}_{n+1}$ is indeed the closest point to $\boldsymbol{\varphi}_{n+1}^{\mathrm{pre}}$ within C in the sense of the kinetic norm (28). It bears emphasis, however, that the closest-point projection onto a non-convex set is set-valued in general and that, consequently, the solution deformation mapping $\boldsymbol{\varphi}_{n+1}$ may be non-unique. This is in contrast to closest-point return mapping algorithms of plasticity, in which the closest-point projection is uniquely determined by virtue of the convexity of the elastic domain.

4. THE VARIATIONAL PRINCIPLE AS A SELECTION CRITERION

The theoretical advantage of the variational approach to contact, especially as regards the *selection* of trajectories in problems where multiple trajectories are possible, may be illustrated through a simple example due to Truesdell [74]. The problem concerns a particle which strikes the tip of a solid wedge at an acute angle, as shown in Figure 1, and reflects off the tip after undergoing a frictionless collision. As it turns out, linear momentum balance alone does not determine a unique trajectory of the particle, which can equally well reflect on either side of the wedge. The problem is to determine, by some rational selection criterion, the most likely—or *preferred*–trajectory of the particle.

Approaches based on re-interpretations of linear momentum balance or on taking the limit of smooth problems have proven relatively unsuccessful at resolving or mitigating the lack of

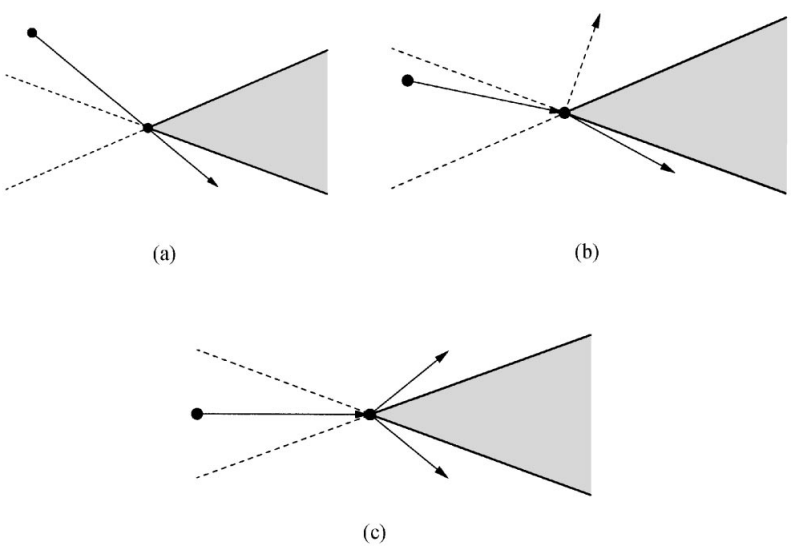

Figure 1. Truesdell's problem of a particle striking the tip of a wedge. Trajectories selected by the variational principle: (a) case 1: grazing trajectory; (b) case 2: shallowest trajectory; (c) case 3: non-unique case.

uniqueness just described. For instance, it is clear that rounding off the tip of the wedge by fitting a smooth curve and subsequently shrinking the curve to a point results in a wide fan of possible scattered directions depending on the precise shape of the curve. This ambiguity may explain why algorithms based on smooth geometry tend to break down when corners are present. By way of contrast, the minimum principle ((29) and (30)) has the virtue of selecting a unique trajectory, excepting the case in which the possible scattered trajectories are indistinguishable by symmetry.

In Truesdell's example the admissible region C is the complement of the wedge, and the objective function is the kinetic distance (28). The three cases which arise are depicted in Figure 1. In case (a), the predictor position of the particle at the end of the time step lies outside the wedge and is, therefore, admissible. The trajectory of the particle grazes the tip and is not deflected. In case (b), the predictor position lies within the wedge and must be projected onto C. For a particle the kinetic distance (28) is equivalent to the Euclidean distance, and hence the requisite projection is onto the closest point of the boundary of the wedge. Two projections are possible, each on either flank of the wedge, a manifestation of the lack of convexity of C. Each of these projections corresponds to the scattering of the particle on either side of the wedge and satisfies linear momentum balance in the sense of (23). However, a strict interpretation of the minimum principle (30) commands us to choose the absolute minimizer, i.e., that position on boundary of the wedge for which the distance to the predictor is smallest. Thus, the variational principle selects the *shallowest* of the two possible scattered trajectories, Figure 1(b). In case (c), the two scattered trajectories are truly equivalent by symmetry and the variational principle is unable to resolve the indeterminacy.

The absolutely continuous trajectories obtained from the time-discretized formulation by passing to the limit of $\triangle t \to 0$ may be interpreted as weak solutions of the equations of motion (8). Truesdell's example reveals that, while in configuration space the solutions are continuous functions of the initial conditions, in phase space the velocity may jump discontinuously and the continuity on the initial conditions is lost.

5. FRICTIONAL CONTACT

Next we turn our attention to situations in which the contact interactions are frictional in nature. In the presence of friction, the force system in Equation (8) has to be extended to include a frictional force field $\mathbf{f}^{\text{fri}}$, whereupon (8) becomes

$$\mathbf{0} \in \mathbf{M}\ddot{\boldsymbol{\varphi}} + \mathbf{f}^{\text{int}}(\boldsymbol{\varphi}) + \partial I_C(\boldsymbol{\varphi}) + \mathbf{f}^{\text{fri}} - \mathbf{f}^{\text{ext}} \tag{31}$$

The frictional forces $\mathbf{f}^{\text{fri}}$ are required to be self-equilibrated and tangential to the surfaces in contact. The former condition ensures that the frictional forces do no work when the bodies are translated, whereas the latter condition ensures that the frictional forces do no work under conditions of normal separation of the bodies. Furthermore, we assume that the magnitude of the frictional forces depends on the normal pressure through a suitable friction law.

These and other restrictions render the formulation of frictional force systems a non-trivial undertaking, specially in finite deformations. We devote the remainder of this section to this problem. For convenience, we shall assume throughout that the admissible set has been characterized through a set of algebraic constraints of form (12).

5.1. Sliding velocity field

The key step in the definition of proper frictional forces is the introduction of the *sliding velocity field*. Let $\dot{\boldsymbol{\varphi}}_\alpha$ be the local velocity field corresponding to the contact constraint α. Thus, $\dot{\boldsymbol{\varphi}}_\alpha$ is the collection of velocities of the nodes contained in the pair of simplices involved in constraint α. Evidently, the local velocity field $\dot{\boldsymbol{\varphi}}_\alpha$ may include rigid-body components and may also contain normal opening or closure modes. We obtain the corresponding local sliding velocity field $\dot{\boldsymbol{\varphi}}_\alpha^{\mathrm{sli}}$ from the full local velocity field $\dot{\boldsymbol{\varphi}}_\alpha$ by removing from the latter its rigid and normal components. Thus, $\dot{\boldsymbol{\varphi}}_\alpha^{\mathrm{sli}}$ follows as the solution of the following problem:

$$\dot{\boldsymbol{\varphi}}_\alpha^{\mathrm{sli}} = \dot{\boldsymbol{\varphi}}_\alpha - \mathbf{c}_\alpha - \boldsymbol{\beta}_\alpha \times \boldsymbol{\varphi}_\alpha - \lambda_\alpha \nabla g_\alpha \tag{32}$$

$$\mathscr{R}(\mathbf{M}_\alpha \dot{\boldsymbol{\varphi}}_\alpha^{\mathrm{sli}}) = \mathbf{0} \tag{33}$$

$$\mathscr{M}(\mathbf{M}_\alpha \dot{\boldsymbol{\varphi}}_\alpha^{\mathrm{sli}}; \boldsymbol{\varphi}_\alpha) = \mathbf{0} \tag{34}$$

$$\mathbf{N}_\alpha \cdot \dot{\boldsymbol{\varphi}}_\alpha^{\mathrm{sli}} = 0 \tag{35}$$

Here, $\mathbf{M}_\alpha$ is the local stiffness matrix, $\mathbf{c}_\alpha$ is an unknown constant vector describing a rigid translation, $\boldsymbol{\beta}_\alpha$ is an unknown angular velocity, and here λ_α is a normal separation velocity. In addition, the operators $\mathscr{R}$ and $\mathscr{M}$ return the resultant and resultant moment of the local vector field which they are applied to, respectively. Evidently, in (32) $\mathbf{c}_\alpha + \boldsymbol{\beta}_\alpha \times \boldsymbol{\varphi}_\alpha$ is a general rigid velocity field, whereas $\lambda_\alpha \nabla g_\alpha$ represents a normal separation velocity field between the two simplices in contact.

Conditions (33) and (34) require that the sliding velocity field have zero total linear and angular momentum. In this sense, the sliding velocity field may be regarded as a *deformation* mode, since it vanishes identically under rigid-body motions. Equation (35) enforces the requirement that $\dot{\boldsymbol{\varphi}}_\alpha^{\mathrm{sli}}$ correspond to pure relative sliding without separation of the simplices in contact. This latter condition in turn ensures that the normal contact forces do no work on the sliding velocities. In view of (13), the orthogonality constraint (35) may alternatively be expressed as

$$\nabla g_\alpha(\boldsymbol{\varphi}_\alpha) \cdot \dot{\boldsymbol{\varphi}}_\alpha^{\mathrm{sli}} = 0 \tag{36}$$

which shows that the constraint function g_α is left invariant by the sliding velocity field, as required. From the linearity of Equations (32)–(35) it follows that $\dot{\boldsymbol{\varphi}}_\alpha^{\mathrm{sli}}$ and $\dot{\boldsymbol{\varphi}}_\alpha$ are linearly related as

$$\dot{\boldsymbol{\varphi}}_\alpha^{\mathrm{sli}} = \mathbf{P}_\alpha(\boldsymbol{\varphi}_\alpha)\dot{\boldsymbol{\varphi}}_\alpha \tag{37}$$

It also follows that $\mathbf{P}_\alpha(\boldsymbol{\varphi}_\alpha)$ is a projection which extracts the local sliding velocity field from the full local velocity fields. Details of the computation of the sliding velocity are given in Appendix B.

5.2. Frictional forces

We may now introduce the local frictional force system $\mathbf{R}_\alpha$ by postulating the existence of a frictional dissipation potential $\psi_\alpha^*(\dot{\boldsymbol{\varphi}}_\alpha; \boldsymbol{\varphi}_\alpha)$ with the property that

$$\mathbf{R}_\alpha = -\partial_{\dot{\boldsymbol{\varphi}}_\alpha} \psi_\alpha^*(\dot{\boldsymbol{\varphi}}_\alpha; \boldsymbol{\varphi}_\alpha) \tag{38}$$

where the dependence of ψ_α^* on $\boldsymbol{\varphi}_\alpha$ is regarded as parametric. In order that $\psi_\alpha^*(\dot{\boldsymbol{\varphi}}_\alpha; \boldsymbol{\varphi}_\alpha)$ represent a true frictional dissipation function, ψ^* can depend on $\dot{\boldsymbol{\varphi}}_\alpha$ only through the sliding velocity field $\dot{\boldsymbol{\varphi}}_\alpha^{\mathrm{sli}}$, i.e.

$$\psi_\alpha^* = \psi_\alpha^*(\dot{\boldsymbol{\varphi}}_\alpha^{\mathrm{sli}}; \boldsymbol{\varphi}_\alpha) \tag{39}$$

For instance, in the particular case of Coulomb's law, the frictional dissipation potential is

$$\psi_\alpha^*(\dot{\boldsymbol{\varphi}}_\alpha; \boldsymbol{\varphi}_\alpha) = \sum_{\text{nodes}} \mu |\mathbf{N}_\alpha(\boldsymbol{\varphi}_\alpha)| |\dot{\boldsymbol{\varphi}}_\alpha^{\mathrm{sli}}| \tag{40}$$

where μ is the coefficient of friction and the sum extends over the nodes of the pair of boundary simplices involved in the contact constraint α.

A dual picture may be obtained by introducing the frictional complementary potential

$$\psi_\alpha(\mathbf{R}_\alpha; \boldsymbol{\varphi}_\alpha) = \min_{\dot{\boldsymbol{\varphi}}_\alpha} \{\mathbf{R}_\alpha \cdot \dot{\boldsymbol{\varphi}}_\alpha - \psi_\alpha^*(\dot{\boldsymbol{\varphi}}_\alpha; \boldsymbol{\varphi}_\alpha)\} \tag{41}$$

To be assured that this Legendre transform is well behaved, we shall henceforth assume that ψ_α^* is a convex function of $\dot{\boldsymbol{\varphi}}_\alpha^{\mathrm{sli}}$. In addition, by virtue of property (39), for problem (41) to have solutions the local frictional force fields $\mathbf{R}_\alpha$ must be orthogonal to all local rigid-body and separation velocity fields. Hence, the local frictional forces must satisfy the constraints

$$\mathscr{R}(\mathbf{R}_\alpha) = \mathbf{0} \tag{42}$$

$$\mathscr{M}(\mathbf{R}_\alpha; \boldsymbol{\varphi}_\alpha) = \mathbf{0} \tag{43}$$

$$\mathbf{R}_\alpha \cdot \nabla g_\alpha(\boldsymbol{\varphi}_\alpha) = 0 \tag{44}$$

which ensure that $\mathbf{R}_\alpha$ is in equilibrium and is orthogonal to the normal forces, as required. By the properties of the Legendre transform applied to convex functions it follows that the frictional dissipation potential is recovered as

$$\psi_\alpha^*(\dot{\boldsymbol{\varphi}}_\alpha; \boldsymbol{\varphi}_\alpha) = \min_{\mathbf{R}_\alpha} \{\mathbf{R}_\alpha \cdot \dot{\boldsymbol{\varphi}}_\alpha - \psi_\alpha(\mathbf{R}_\alpha; \boldsymbol{\varphi}_\alpha)\} \tag{45}$$

In addition, we have

$$\dot{\boldsymbol{\varphi}}_\alpha^{\mathrm{sli}} = \partial_{\mathbf{R}_\alpha} \psi_\alpha(\mathbf{R}_\alpha; \boldsymbol{\varphi}_\alpha) \tag{46}$$

i.e. ψ_α acts as a potential for the sliding local velocity field.

It is interesting to note that, as a consequence of constraints (42)–(44), it follows that

$$\mathbf{R}_\alpha \cdot \dot{\boldsymbol{\varphi}}_\alpha = \mathbf{R}_\alpha \cdot \dot{\boldsymbol{\varphi}}_\alpha^{\mathrm{sli}} \tag{47}$$

i.e. the frictional forces do work on the sliding velocities only. These duality relations are in analogy to those which pertain to stresses and strains, and nodal forces and nodal displacements in a conventional finite element context. In particular, the sliding local velocity field $\dot{\boldsymbol{\varphi}}_\alpha^{\mathrm{sli}}$, which vanishes for local rigid-body motions, plays the role of a deformation rate, and the local frictional forces $\mathbf{R}_\alpha$ play the role of the conjugate stresses.

The particular case of Coulomb's law of friction is noteworthy. In this case, the frictional complementary potential is

$$\psi_\alpha(\mathbf{R}_\alpha;\boldsymbol{\varphi}_\alpha)=\begin{cases}0 & \text{if } \begin{cases}|\mathbf{R}_\alpha|\leqslant\mu|\mathbf{N}_\alpha(\boldsymbol{\varphi}_\alpha)| \text{ for all local nodes}\\ \mathbf{R}_\alpha \text{ satisfies constraints (42)–(44)}\end{cases}\\ \infty & \text{otherwise}\end{cases} \tag{48}$$

and the frictional forces follow (38) in the form

$$\mathbf{R}_\alpha=\mu|\mathbf{N}_\alpha(\boldsymbol{\varphi}_\alpha)|\mathbf{P}_\alpha^{\mathrm{T}}\,\dot{\boldsymbol{\varphi}}_\alpha^{\mathrm{sli}}/|\dot{\boldsymbol{\varphi}}_\alpha^{\mathrm{sli}}| \quad \text{if } \dot{\boldsymbol{\varphi}}_\alpha^{\mathrm{sli}}\neq\mathbf{0} \tag{49a}$$

$$\mathbf{R}_\alpha\in\{\mathbf{F}_\alpha \text{ s.t. } |\mathbf{F}_\alpha|\leqslant\mu|\mathbf{N}_\alpha(\boldsymbol{\varphi}_\alpha)| \text{ for all local nodes}\} \quad \text{if } \dot{\boldsymbol{\varphi}}_\alpha^{\mathrm{sli}}=\mathbf{0} \tag{49b}$$

These relations apply node by node. The first case corresponds to *slip* conditions, whereas the second case corresponds to *stick*. In this latter case, the frictional forces are not determined uniquely by Coulomb's law and follow from equilibrium.

The global frictional force array $\mathbf{f}^{\mathrm{fri}}$ may be obtained by assembly of all the local frictional forces arrays $\mathbf{R}_\alpha$, i.e.

$$\mathbf{f}^{\mathrm{fri}}=\mathscr{A}(\{\mathbf{R}_\alpha,\ \alpha=1,\ldots,N\}) \tag{50}$$

We note that, since all the local velocity arrays derive from a compatible global velocity fields, we have the identities

$$\sum_{\alpha=1}^{N}\mathbf{R}_\alpha\cdot\dot{\boldsymbol{\varphi}}_\alpha=\mathbf{f}^{\mathrm{fri}}\cdot\dot{\boldsymbol{\varphi}} \tag{51}$$

This relation in turn implies that the global frictional force field $\mathbf{f}^{\mathrm{fri}}$ inherits the potential structure from the local fields, i.e.

$$\mathbf{f}^{\mathrm{fri}}=-\partial_{\dot{\boldsymbol{\varphi}}}\psi^*(\dot{\boldsymbol{\varphi}};\boldsymbol{\varphi}) \tag{52}$$

where

$$\psi^*(\dot{\boldsymbol{\varphi}};\boldsymbol{\varphi})=\sum_{\alpha=1}^{N}\psi_\alpha^*(\dot{\boldsymbol{\varphi}}_\alpha;\boldsymbol{\varphi}_\alpha) \tag{53}$$

is the global frictional dissipation function.

6. TIME-DISCRETIZATION: FRICTIONAL CONTACT

Our aim now is to extend the variational framework of Section 3 to the frictional case. The device which we employ in order to make such variational characterization possible is time-discretization. The fact that time-discretization opens an avenue for the definition of minimum principles for dissipative problems has been pointed out only recently [66, 64, 67]. This technique has also been applied to problems involving dissipation of the Rayleigh type in Reference [75].

Following References [66, 64, 67, 75], we extend the variational principles ((29) and (30)) by the addition to the objective function of an incremental or time-discretized frictional dissipation, with the result

$$f(\boldsymbol{\varphi}_{n+1}) = \|\boldsymbol{\varphi}_{n+1} - \boldsymbol{\varphi}_{n+1}^{\text{pre}}\|_K^2 + 2\beta[\phi(\boldsymbol{\varphi}_{n+1}) - \mathbf{f}_{n+1}^{\text{ext}} \cdot \boldsymbol{\varphi}_{n+1}] + \triangle t \psi^* \left(\frac{\boldsymbol{\varphi}_{n+1} - \boldsymbol{\varphi}_n}{\triangle t}; \boldsymbol{\varphi}_{n+1} \right) \tag{54}$$

Other than this extension, the minimum principles ((29) and (30)) remain in force. We note in passing that, using (45), it is also possible to formulate a min-max variational principle jointly in the deformation mapping $\boldsymbol{\varphi}_{n+1}$ and the frictional forces $\mathbf{R}_{n+1}$, but this avenue will not be pursued here.

It should be noted that the incremental frictional dissipation in (54) is based on a simple divided-difference approximation of the velocity, and that this approximation is introduced independently of the Newmark relations. In this manner, the discretization of the frictional dissipation retains its meaning in the static case. Other discretizations of the frictional dissipation which rely on the Newmark velocities are also possible, but will not be pursued here. We also note that the variational principle just formulated is necessarily incremental, even in the static case, as required by the dissipative nature of friction. In particular, the formulation allows for hysteresis upon cyclic loading.

The Euler–Lagrange equations corresponding to the objective function (54) are

$$\mathbf{0} \in \frac{2}{\triangle t^2}\mathbf{M}(\boldsymbol{\varphi}_{n+1} - \boldsymbol{\varphi}_{n+1}^{\text{pre}}) + 2\beta[\mathbf{f}^{\text{int}}(\boldsymbol{\varphi}_{n+1}) - \mathbf{f}_{n+1}^{\text{ext}}] + \partial I_C(\boldsymbol{\varphi}_{n+1}) + \mathbf{f}_{n+1}^{\text{fri}} \tag{55}$$

Here the frictional forces follow as

$$\begin{aligned} \mathbf{f}_{n+1}^{\text{fri}} &= -\frac{\partial}{\partial \boldsymbol{\varphi}_{n+1}} \left[\triangle t \psi^* \left(\frac{\boldsymbol{\varphi}_{n+1} - \boldsymbol{\varphi}_n}{\triangle t}; \boldsymbol{\varphi}_{n+1} \right) \right] \\ &= -\delta_1 \psi^* \left(\frac{\boldsymbol{\varphi}_{n+1} - \boldsymbol{\varphi}_n}{\triangle t}; \boldsymbol{\varphi}_{n+1} \right) - \triangle t \delta_2 \psi^* \left(\frac{\boldsymbol{\varphi}_{n+1} - \boldsymbol{\varphi}_n}{\triangle t}; \boldsymbol{\varphi}_{n+1} \right) \end{aligned} \tag{56}$$

which is clearly consistent with the frictional law (52) up to admissible truncation errors. In view of this consistency, it follows that Equation (55) itself furnishes a consistent time discretization of the full equations of motion (31). The full displacement and velocity updates then follows from (19) and (20), with the accelerations computed from (17) and (18). Observe however that in this latter equation the full contact forces are now given by

$$\mathbf{f}_{n+1}^{\text{con}} = \partial I_C(\boldsymbol{\varphi}_{n+1}) + \mathbf{f}_{n+1}^{\text{fri}} \tag{57}$$

These expressions close the algorithm.

A subtle point concerning the algorithmic frictional force in (56) requires careful attention. Thus, a comparison of this expression with (52) reveals that, in taking the full gradient of $\triangle t \psi^*$ with respect to $\boldsymbol{\varphi}_{n+1}$ we pick up the additional term $\triangle t \delta_2 \psi^*$ not present in (52). For instance, in Coulomb's model (40) this spurious term arises from the differentiation of the dependence of ψ^* on $\boldsymbol{\varphi}_{n+1}$ introduced by (a) the projection of the local velocity fields onto their sliding components and (b) the normal contact forces. However, it should be noted that the spurious second order term in (56) is of order $O(\triangle t)$, and can therefore be regarded as an admissible contribution to the truncation error of the algorithm. In this manner Coulomb's

law of friction can be formulated in variational form as a minimum principle, despite its 'non-associated' character.

7. ILLUSTRATIVE EXAMPLES

The nature of the variational formulation of frictional contact just developed may be illustrated by way of the simple but illuminating example of a particle striking a flat plate. The frictional force is assumed to obey Coulomb's law of friction. In particular, we endeavour to demonstrate how, by the structure of the objective function (54) and Coulomb's dissipation potential (40), the variational principle properly accounts for stick and slip conditions.

The plate is rigid and occupies the half-space $y \leqslant 0$, Figure 2(a). The trajectory of the particle is in the x–y plane. For simplicity, we assume that the particle is in contact with the plate at time t_n and take $\beta = 0$. The case in which the particle is initially offset from the plate may be treated by a method of fractional steps in which the time step is split into free-flight and contact sub-steps. The analysis that follows then applies to the contact sub-step.

Since friction operates in the direction tangential to the plate only, the normal reaction is independent of the coefficient of friction and follows as

$$N = \frac{2m}{\triangle t^2}|y_{n+1} - y_{n+1}^{\text{pre}}| = \frac{2m}{\triangle t^2}(y_{n+1} - y_{n+1}^{\text{pre}}) \tag{58}$$

where

$$y_{n+1}^{\text{pre}} = y_n + \triangle t \dot{y}_n < 0 \tag{59}$$

is the unconstrained predictor. The sliding velocity coincides with the tangential component of the particle velocity, namely,

$$\dot{x}_{n+1}^{\text{sli}} = \dot{x}_{n+1} \tag{60}$$

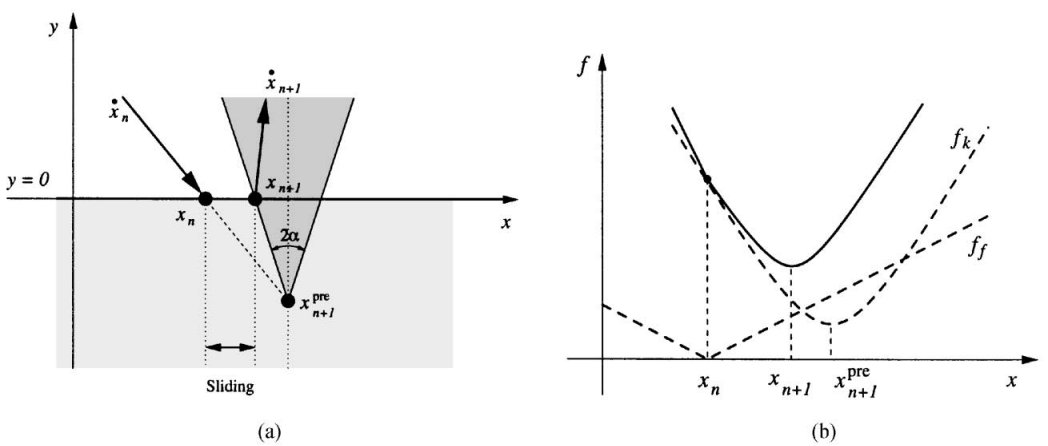

Figure 2. Collision of a particle and a rigid plate, slip case: (a) schematic of the algorithm; (b) objective function (solid line) and contributions from friction (dashed line, f_f) and inertia (dashed line, f_k).

Using Equations (58)–(60), the dissipation potential becomes

$$\psi^*(\dot{x}_{n+1}, y_{n+1}) = \mu \frac{2m}{\triangle t^2}(y_{n+1} - y_{n+1}^{\text{pre}})|\dot{x}_{n+1}| \tag{61}$$

where we discretize the sliding velocity as

$$\dot{x}_{n+1} = \frac{x_{n+1} - x_n}{\triangle t} \tag{62}$$

Inserting Equations (61) and (62) into (54), we obtain

$$f = \frac{m}{\triangle t^2}[(x_{n+1} - x_{n+1}^{\text{pre}})^2 + (y_{n+1} - y_{n+1}^{\text{pre}})^2 + 2\mu(y_{n+1} - y_{n+1}^{\text{pre}})|x_{n+1} - x_n|] \tag{63}$$

This function comprises two terms: a quadratic term contributed by inertia; and a *cone* contributed by friction. The sum of these two terms is convex but nonsmooth, owing to the presence of the term $|x_{n+1} - x_n|$, Figure 2(b). In particular, the function f has a vertex at $x_{n+1} = x_n$. It should be emphasized that the lack of smoothness of f is entirely due to friction. The constrained minimization problem (30) leads to the equations

$$y_{n+1} = 0, \quad x_{n+1} - x_{n+1}^{\text{pre}} + \mu(y_{n+1} - y_{n+1}^{\text{pre}})\frac{x_{n+1} - x_n}{|x_{n+1} - x_n|} = 0 \tag{64}$$

where we tacitly assume that $x_{n+1} \geqslant x_n$.

The solutions fall into two categories, depending on whether the kinetic or the frictional contribution to the objective function f dominates:

Slip: In this case, the quadratic kinetic term in (63) dominates and the minimum of f is attained away from x_n, Figure 2(b), with the result

$$y_{n+1} = 0, \quad x_{n+1} = x_{n+1}^{\text{pre}} + \mu y_{n+1}^{\text{pre}} \tag{65}$$

Referring to Figure 2(a), we note that the final position of the particle is on the surface of Coulomb's cone. The value of the frictional force follows from (49a) as

$$R = -\mu \frac{2m}{\triangle t^2} y_{n+1}^{\text{pre}} > 0 \tag{66}$$

The tangential acceleration and velocity are given by

$$\ddot{x}_{n+1} = \frac{2}{\triangle t^2}(x_{n+1} - x_{n+1}^{\text{pre}}) = \mu \frac{2}{\triangle t^2} y_{n+1}^{\text{pre}} \leqslant 0 \tag{67}$$

$$\dot{x}_{n+1} = \dot{x}_n + \triangle t \ddot{x}_{n+1} = \dot{x}_n + \mu \frac{2}{\triangle t} y_{n+1}^{\text{pre}} \leqslant \dot{x}_n \tag{68}$$

We note that friction tends to decelerate the particle in the direction of sliding, as expected.

Figure 3(a) shows the plot of the final tangential velocity versus the friction coefficient μ. The tangential velocity vanishes for the coefficient of friction

$$\mu^0 = -\frac{\triangle t \dot{x}_n}{2 y_{n+1}^{\text{pre}}} \tag{69}$$

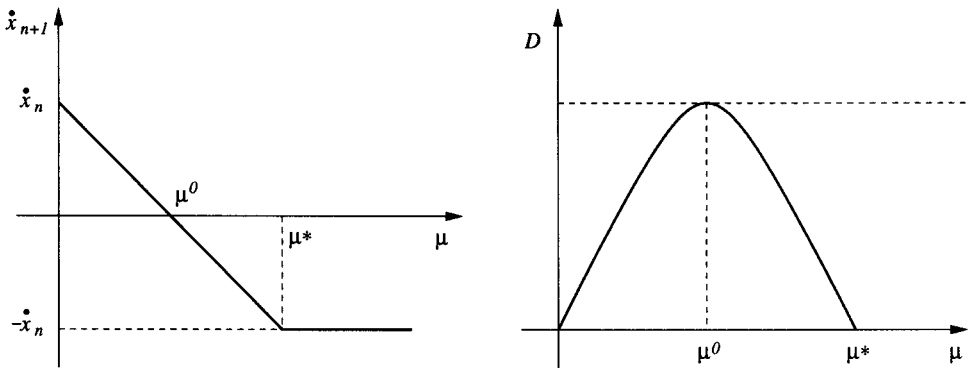

Figure 3. (a) Final tangential velocity versus μ; (b) dissipation versus μ.

and is negative for $\mu > \mu^0$. The final velocity reverses fully for the coefficient of friction

$$\mu^* = -\frac{\triangle t \dot{x}_n}{y_{n+1}^{\text{pre}}} = 2\mu^0 \tag{70}$$

corresponding to $x_{n+1} = x_n$. The variation $\triangle K$ in kinetic energy is

$$\triangle K = \mu \frac{2m}{\triangle t} \dot{x}_n y_{n+1}^{\text{pre}} + \mu^2 \frac{2m}{\triangle t^2} y_{n+1}^{\text{pre2}} = \mu \frac{2m}{\triangle t^2} y_{n+1}^{\text{pre}} (\triangle t \dot{x}_n + \mu y_{n+1}^{\text{pre}}) \leqslant 0 \tag{71}$$

which corresponds to a net loss of kinetic energy as expected. The frictional dissipation, on the other hand, follows as

$$D = R_{x,n+1}(x_{n+1} - x_n) = -\mu \frac{2m}{\triangle t^2} y_{n+1}^{\text{pre}} (\triangle t \dot{x}_n + \mu y_{n+1}^{\text{pre}}) \geqslant 0 \tag{72}$$

We note that $D + \triangle K = 0$, as required by conservation of energy. The dependence of the residual tangential velocity and energy loss on the coefficient of friction are shown in Figure 3. The maximum dissipation is obtained for $\mu = \mu^0$, for which the final tangential velocity is zero. The dissipation vanishes as $\mu \to 0$ or $\mu \to \mu^*$.

Stick: In this case, the frictional component of the objective function f dominates, Figure 4(b), and its minimum is attained at the vertex of the cone, or $x_{n+1} = x_n$. The final position of the particle is inside the friction cone, Figure 4(a). Stick occurs in a limit case of slip attained as $\mu \to \mu^*$, which, as noted above, in turn results in a fully reversed velocity and no dissipation, and it occurs for all $\mu \geqslant \mu^*$. The frictional force follows as

$$R^{\text{stick}} = \mu^* N = \frac{2m\dot{x}_n}{\triangle t} \leqslant -\mu \frac{2m}{\triangle t^2} y_{n+1}^{\text{pre}} \tag{73}$$

which satisfies the Coulomb bound, as required.

The above solutions are in keeping with the expected behaviour of the system, which provides a first verification of the proposed variational principle. We particularly emphasize

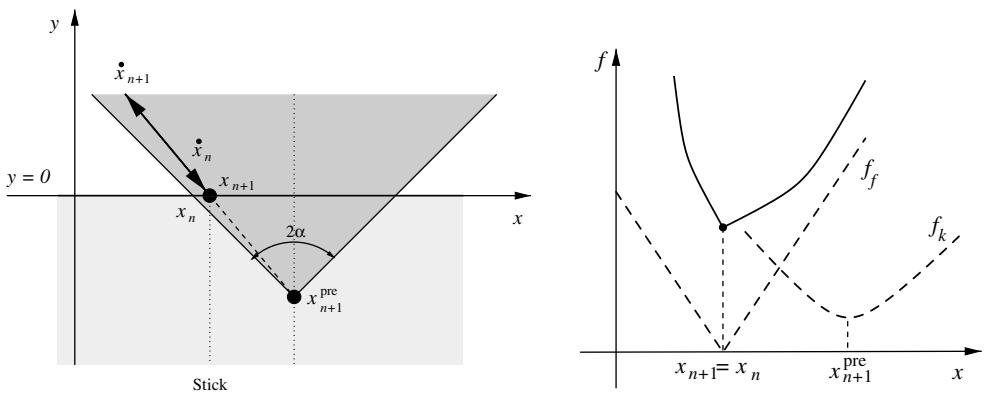

Figure 4. Collision of a particle and a rigid plate, stick case: (a) schematic of the algorithm; (b) objective function (solid line) and contributions from friction (dashed line, f_f) and inertia (dashed line, f_k).

the ability of the formulation to predict stick–slip behaviour. It is interesting to note that the frictional force (73) diverges as $\triangle t \to 0$. However, the work of friction remains bounded throughout. In addition, the computed relation between the incoming and outgoing velocities is independent of $\triangle t$ and, therefore, remains unchanged in the limit of $\triangle t \to 0$. Conversely, the finite $\triangle t$ case may be regarded as a regularization of the continuous formulation.

8. NUMERICAL EXAMPLES

In this section, we collect the results of selected numerical tests which demonstrate the robustness and versatility of the algorithms previously described. In all calculations, the bodies are modelled as finitely deforming elastic materials obeying a Neo-Hookean constitutive law extended to the compressible range. The assumed strain energy density has the form

$$W(\mathbf{F}) = \frac{\lambda_0}{2}(\log J)^2 - \mu_0 \log J + \frac{\mu_0}{2}\,\mathrm{tr}(\mathbf{C}) \tag{74}$$

where $\mathbf{F} = \nabla_0 \boldsymbol{\varphi}$ is the deformation gradient; $\mathbf{C} = \mathbf{F}^{\mathrm{T}}\mathbf{F}$ is the right Cauchy–Green deformation tensor; $J = \det(F)$ is the Jacobian of the deformation; and λ_0 and μ_0 are material constants. The finite-element implementation of this model accounts for full finite-deformation kinematics, which allows the bodies to deform, translate and rotate freely. The particular choice of material constants used in calculations is: $\lambda_0 = 115.4\,\mathrm{GPa}$, $\mu_0 = 79.6\,\mathrm{GPa}$ and a referential mass density $\rho_0 = 7,800\,\mathrm{kg/m^3}$. All calculations are carried out using the explicit algorithm, $\beta = 0$. The time step is chosen as a fraction of the stable time step for explicit integration. The constrained minimization problem (30) is solved using Spellucci's implementation of sequential quadratic programming [71].

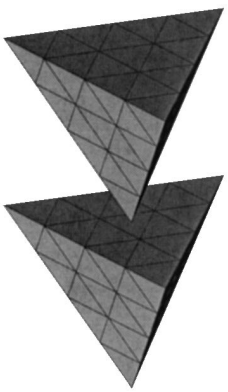

Figure 5. Vertex on face collision of two tetrahedra. Computational mesh and initial configuration.

8.1. Collisions between tetrahedra

As a first example of a non-smooth contact, we consider the case of the collision between two regular deformable tetrahedra. Owing to the sharp edges and vertices of the tetrahedra, the calculations demonstrate the non-smooth characteristics of the algorithm. A first configuration concerns a tetrahedron one of whose vertices strikes the face of a second tetrahedron. The two tetrahedra have the same volume and mass. The mesh, comprising 70 nodes and 16 elements, and the configuration at the point of impact are depicted in Figure 5. Both tetrahedra are unconstrained. Prior to impact the top tetrahedron translates rigidly with velocity $v_x = 0.21\,\text{mm}/\mu\text{s}$, $v_y = 0$ and $v_z = -0.21\,\text{mm}/\mu\text{s}$, whereas the second tetrahedron is at rest. The friction coefficient μ is given values ranging from 0 to 1.

The frictionless collision, $\mu = 0$, is shown in Figure 6. Figure 6(a) shows the linear momentum history; Figure 6(b) the angular momentum history; Figure 6(c) the kinetic (K), elastic (U) and the total ($K + U$) mechanical energy history; and Figure 6(d) depicts the trajectory of the node closest to the centroid of the top tetrahedron. The first three figures clearly demonstrate the good energy-momentum conservation properties of the algorithm. In particular, Figure 6(c) shows the exchange between kinetic and elastic energy during the contact phase; both energies recover their initial value after the collision phase. Figure 6(d) illustrates how the trajectory of the top tetrahedron is deflected as a result of the collision. In particular we see how the top tetrahedron exchanges the vertical or normal component of its linear momentum with the bottom tetrahedron, conserving at the same time the horizontal or tangential component.

Results for the corresponding frictional cases are collected in Figure 7. We observe in this figure that the total mechanical energy decays monotonically in time, Figure 7(a), and that the dissipation rate increases with the coefficient of friction. In the presence of friction, the trajectories of the centroid of the top tetrahedron, Figure 7(b), are in marked contrast to the frictionless trajectories. Thus, the top tetrahedron catches at its tip and transfers tangential momentum to the bottom tetrahedron. As a consequence of this frictional interaction, both tetrahedra acquire angular momentum and start to rotate.

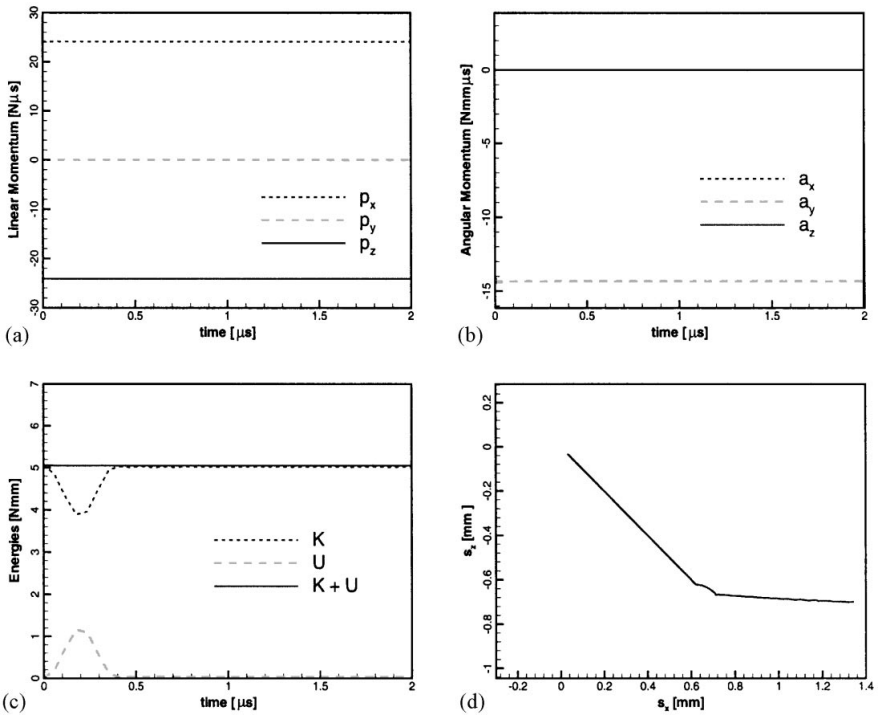

Figure 6. Non-smooth frictionless vertex-on-face collision of two unconstrained tetrahedra: (a) linear momentum history; (b) angular momentum history; (c) evolution of elastic, kinetic and total energy; (d) trajectory of a node close to the centroid of the top tetrahedron.

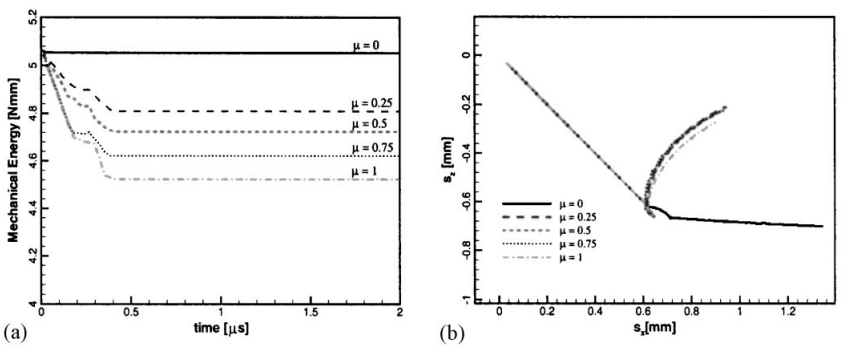

Figure 7. Non-smooth frictional vertex-to-face collision of two unconstrained tetrahedra: (a) total mechanical energy histories for different values of the friction coefficient; (b) trajectories of a node close to the centroid of the top tetrahedron for different values of the friction coefficient.

As a second example, we consider the face-on-face collision between two tetrahedra. The properties and geometry of the tetrahedra are as in the preceding example. The initial configuration of the bodies is shown in Figure 8. Both tetrahedra are unconstrained. Prior to impact, the top tetrahedron has an initial velocity $v_x = 0.21$ mm/μs, $v_y = 0$ and $v_z = -0.21$ mm/μs,

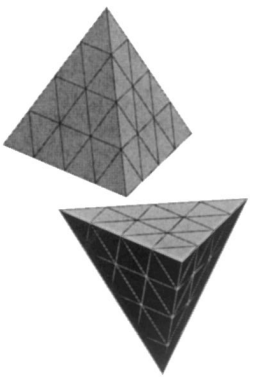

Figure 8. Face on face collision of two tetrahedra. Computational mesh and initial configuration.

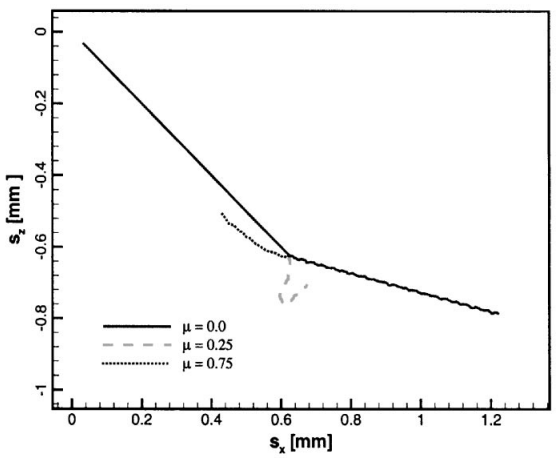

Figure 9. Smooth frictionless and frictional collision of two unconstrained bodies: trajectories of a node close to the centroid of the top tetrahedron for different values of the friction coefficient.

whereas the second tetrahedron is at rest. It should be carefully noted that all eight faces of the two tetrahedra can potentially intersect during the predictor phase of the algorithm, which renders the collision non-smooth. We also note that the two faces which come into contact come into exact coincidence at the point of impact. In particular, their edges collide pairwise. Coincidences of this type can potentially tax the face-on-face intersection algorithm and render the results sensitive to the choice of tolerance.

Figure 9 shows the trajectories of a node close to the centroid of the top tetrahedron for three different values of the friction coefficient, $\mu = 0$, 0.25 and 0.75, respectively. The effect of friction on the trajectories is particularly noteworthy. Thus, an increase in the friction coefficient results in a steady transition from slip to stick. For the highest value of the coefficient of friction considered in the calculations, the velocity of the centre of mass of the incoming tetrahedron fully reverses its direction, and it is a clear manifestation of the occurrence of perfect stick conditions at the contact.

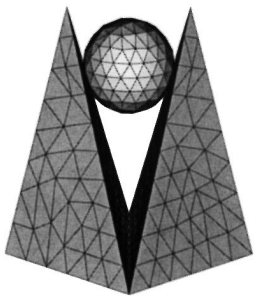

Figure 10. Penetration of a crevice by a sphere: computational mesh.

8.2. Penetration of a crevice by a sphere

Our last example concerns a sphere which penetrates and wedges itself into a crevice formed by two tetrahedra, Figure 10. Prior to impact the sphere undergoes a rigid translation with vertical velocity $v_z = -0.3\,\text{mm}/\mu\text{s}$. The tetrahedra are supported at their bases and are initially at rest. The mesh used in the calculations, comprising 550 nodes and 230 elements, is also shown in Figure 10.

Figure 11 shows selected results for the frictionless case, including histories of linear and angular momentum and energy. Figure 11(d) shows the trajectory of centroid of the sphere. The good conservation properties of the algorithm are evident in these results. As the sphere penetrates the crevice, it undergoes multiple collisions with the two tetrahedra. Simultaneously, the sphere and the tetrahedra undergo finite amplitude vibrations, which accounts for the unsteady appearance of the trajectories.

Figure 12 illustrates the effect of friction for μ ranging between 0.1 to 0.5. The total energy of the system exhibits a steady decay in time, Figure 12(a). Interestingly, as in the simple example of a particle striking a rigid flat plate discussed in Section 7, the maximum frictional dissipation is attained for an intermediate value of $\mu = 0.3$. A comparison between the frictionless trajectory and the trajectory corresponding to $\mu = 0.4$ is shown in Figure 12(b). As may be observed in this figure, the presence of friction causes the penetration depth of the sphere to be considerably less than in the frictionless case and its velocity remarkably lower, so that the final position is lower. This in turn accounts for the non-monotonic dependence of the frictional dissipation on the coefficient of friction. Thus, as μ is initially increased from 0, the frictional dissipation correspondingly increases, as expected. However, the penetration depth also decreases with μ, which tends to reduce the amount of frictional dissipation. For $\mu > 0.3$, this latter effect dominates and the frictional dissipation decreases with increasing μ.

9. SUMMARY AND DISCUSSION

The present work extends the non-smooth contact formulation of Kane *et al.* [1] to the case of friction. In this approach, non-smooth analysis (see Reference [58]) is taken as a basis for the development of contact algorithms capable of dealing with complex contact situations involving multiple bodies with corners. The formulation specifically addresses contact

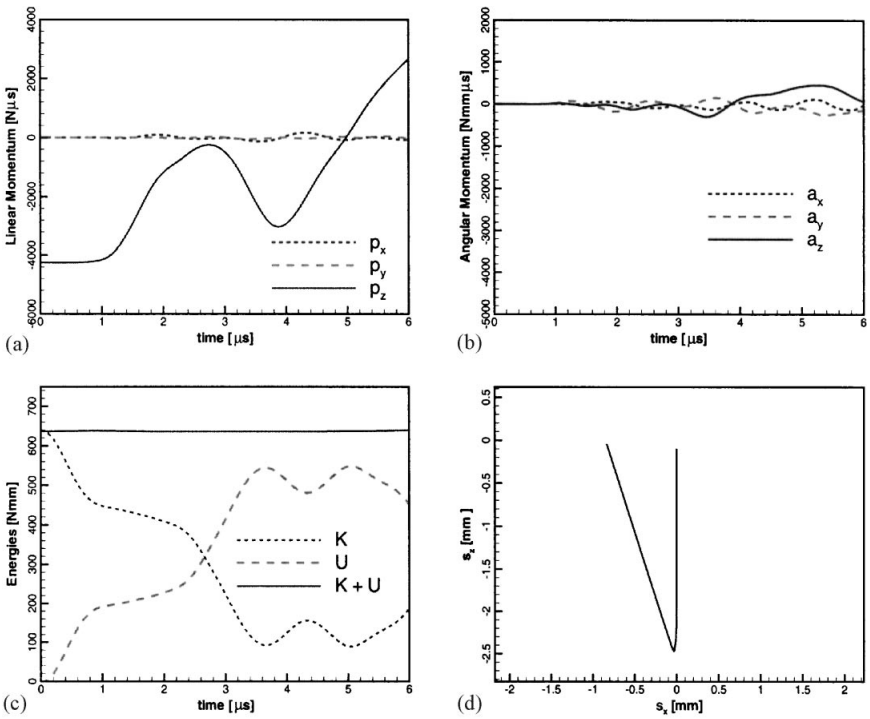

Figure 11. Non-smooth frictionless contact of a sphere penetrating a crevice: (a) linear momentum story; (b) angular momentum story; (c) energies story; (d) trajectory of a node close to the centroid of the sphere.

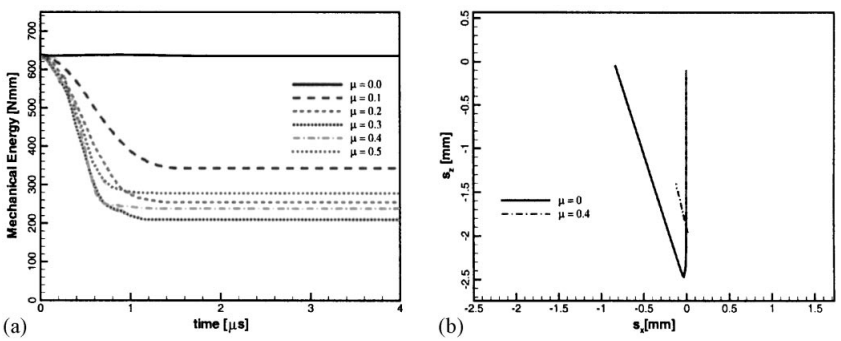

Figure 12. Non-smooth constrained frictional contact of a sphere penetrating a crevice: surfaces: (a) total mechanical energy histories for different values of the friction coefficient; (b) trajectory of a node close to the centroid of the sphere for different values of the friction coefficient.

geometries for which neither normals nor gap functions may be properly defined, which precludes the application of most contact algorithms proposed to date. Such situations arise in applications such as: fragmentation, where angular fragments undergo complex collision sequences before they scatter; granular flows, and others. The formulation accords all bodies

an equal role without differentiating between master and slave bodies. This is particularly advantageous in situations such that several angular bodies meet near a point, as for these configurations it is not generally possible to classify the bodies as master or slave.

A far-reaching aspect of the non-smooth contact algorithm of Kane *et al.* [1] is that the incremental displacements follow from a *minimum* principle. The objective function comprises terms which account for inertia, strain energy, contact and external forcing. As noted by Ortiz and Radovitzky [66], the variational principle at work in Kane *et al.* approach [1] is of a radically different nature than the variational principles of classical mechanics, e.g. Hamilton's principle of stationary action. Thus, while this latter principle pertains to trajectories and constitutes a stationarity principle, the variational principles proposed by Ortiz and Radovitzky [66] for dynamical systems, and by Kane *et al.* [1] for contact dynamics, are *minimum* principles and pertain to the time-discretized incremental problem. In addition to its value as a basis for formulating numerical algorithms, we have shown that this variational framework offers theoretical advantages as regards the *selection* of trajectories in cases of non-uniqueness. We have illustrated this variational selection criterion with the aid of a simple example due to Truesdell [74].

The extension to friction presented here aims first and foremost at retaining the variational structure of the formulation. The ability to do so owes greatly to recent work which has elucidated the connection between—once again—time-discretization and minimum principles for dissipative systems [66, 64, 67]. Within this framework, friction is accounted for simply by adding to the objective function a term which measures the incremental work of friction. The reckoning of the work of friction requires some care, in that the velocity must be projected onto its *sliding* component in order to ensure that translations and normal separation result in no frictional dissipation. We have shown that the Euler–Lagrange equations corresponding to the extended variational principle are indeed consistent with the equations of motion of solids undergoing frictional collisions. It is noteworthy that friction, while being in analogy to the so-called non-associative plasticity rules, is nevertheless amenable to a variational characterization. The possibility of extending the present work on friction to non-associative plasticity in general suggests itself as a worthwhile direction of future research.

Our numerical results are consistent with what is generally known about the conservation properties of the Newmark algorithm. In particular, Kane *et al.* [75] have recently pointed out that the Newmark algorithm has a variational structure in the sense of Veselov and, consequently, it conserves exactly an algorithmic form of the linear and angular momenta. This accounts for the good linear and angular momentum conservation properties exhibited by the non-smooth contact algorithm. However, when Newmark's algorithm is applied with a constant time step, energy is not conserved in general but rather oscillates. This also accounts for the small fluctuations in energy observed in our frictionless examples. Under worst-scenario circumstances, such as in the case of a single particle striking a rigid wall in the middle of a time step, the deviation of the algorithm from energy conservation may be severe. However, as our numerical examples demonstrate, lack of strict energy conservation does not appear to be a significant problem in moderate to large scale computations. In addition, Kane *et al.* have recently pointed out that Newmark's algorithm can be made to conserve energy exactly by allowing the time step to vary in duration. This observation suggests ways to improve the energy conservation characteristics of the present contact algorithm, e.g. by time-step adaption or by recourse to fractional steps. This, too, would appear to be a worthwhile direction of future research.

APPENDIX A: EVALUATION OF THE CONTACT CONSTRAINTS

In this appendix, we collect implementation details pertaining to the evaluation of the contact constraints. The boundaries of the solids are assumed to be triangulated and oriented so as to define their interior and exterior domains unambiguously. Each pair of simplices in the boundary triangulation defines a—possibly inactive—constant constraint. Given a pair of boundary simplices, we wish to define a simple function g of the nodal positions such that $g \geqslant 0$ when the simplices do not interpenetrate and $g < 0$ otherwise. Here we restrict our attention to the three-dimensional case. The constraint functions derived here are somewhat simpler than those proposed by Kane *et al.* [1]. The two-dimensional problem is amenable to a similar treatment. The details of this treatment may be found elsewhere [1].

By convention, all boundary facets are oriented counterclockwise when seen from outside the body, so that the interior of a body is below its boundary. We consider a pair of triangles T_1 and T_2 in space defined by vertices $\{\mathbf{x}_1, \mathbf{x}_2, \mathbf{x}_3\}$ and $\{\mathbf{x}_4, \mathbf{x}_5, \mathbf{x}_6\}$, respectively. The types of intersections between the triangles fall into two distinct categories, Figure A1. The first case occurs when the intersection is fully contained within one of the triangles, Figure A1(a), whereas in the remaining case the intersection abuts on two segments. All possible intersections can be obtained from those shown in Figure A1 by a suitable permutation of the indices. We denote **A** and **B** the two extreme points of the intersection for case (a), and **A** and **C** in case (b), Figure A1. The calculation of these points is a standard problem in computational geometry (see, e.g. Reference [76]).

The extreme points of the intersection (**A** and **B**, **A** and **C** in the first and in the second case, respectively) may be used to define algebraic impenetrability constraints for the two triangles. A set of constraint functions may be based on the volumes of certain tetrahedra, [1]. In the present work, we choose an alternative set of constraint functions derived from the distance between the extreme points of the intersection, namely,

$$g = \pm \|\mathbf{A} - \mathbf{B}\|, \quad \text{case (a)} \tag{A1}$$

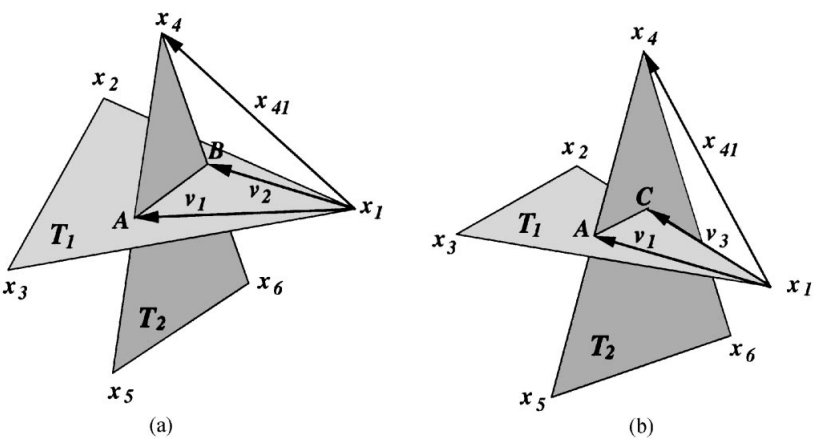

Figure A1. The two types of intersections between triangular facets.

and

$$g = \pm \|\mathbf{A} - \mathbf{C}\|, \quad \text{case (b)} \tag{A2}$$

with the sign chose as negative in the case of intersection and positive otherwise. With this definition, a deformed configuration is in the admissible set C if $g \geqslant 0$ for all distinct pairs of boundary triangles.

APPENDIX B: COMPUTATION OF SLIDING VELOCITIES

In this appendix, we provide explicit expressions for the projection which extracts the sliding component from the velocity field of a pair of simplices. We label $a = 1, \ldots, n$ the nodes of the simplices under consideration. The corresponding nodal co-ordinates are $\mathbf{x}_a$ and the velocities are $\mathbf{v}_a$. The corresponding local sliding velocity field is obtained by removing from $\mathbf{v}_a$ its rigid and normal components, i.e.

$$v_{ia}^{\mathrm{sli}} = v_{ia} - c_i - e_{ijk}\beta_j x_{ka} - \lambda \frac{\partial g}{\partial x_{ia}} \tag{B1}$$

where g is the constraint function defined in Appendix A. The translation velocity $\mathbf{c}$, angular velocity $\boldsymbol{\beta}$, and normal velocity λ follow from the system of equations (where with M_a we denote the nodal mass):

$$\sum_{a=1}^{n} M_a \left\{ -v_{ia} + c_i + e_{ijk}\beta_j x_{ka} + \lambda \frac{\partial g}{\partial x_{ia}} \right\} = 0 \tag{B2}$$

$$\sum_{a=1}^{n} M_a \left\{ e_{imn} \left(-v_{ma} + c_m + e_{mjk}\beta_j x_{ka} + \lambda \frac{\partial g}{\partial x_{ma}} \right) x_{na} \right\} = 0 \tag{B3}$$

$$\sum_{a=1}^{n} \left\{ \frac{\partial g}{\partial x_{ia}} \left(-v_{ia} + c_i + e_{ijk}\beta_j x_{ka} + \lambda \frac{\partial g}{\partial x_{ia}} \right) \right\} = 0 \tag{B4}$$

Since g is translation and rotation invariant, ∇g does not contain translational nor rotational components, and the first two equations in the above system simplify to

$$\sum_{a=1}^{n} M_a \{ -v_{ia} + c_i + e_{ijk}\beta_j x_{ka} \} = 0 \tag{B5}$$

$$\sum_{a=1}^{n} M_a \{ e_{imn}(-v_{ma} + c_m + e_{mjk}\beta_j x_{ka}) x_{na} \} = 0 \tag{B6}$$

The first of these equations gives

$$c_i = \bar{v}_i - e_{ijk}\beta_j \bar{x}_k \tag{B7}$$

where we have introduced the notation

$$\bar{f}_i = \frac{1}{\bar{M}} \sum_{a=1}^{n} M_a f_{ia} \tag{B8}$$

with

$$\bar{M} = \sum_{a=1}^{n} M_a \tag{B9}$$

Substituting (B7) into (B6) gives

$$e_{imn}(e_{mjk}\beta_j\overline{\delta x_k x_n} - \overline{\delta v_m x_n}) = 0 \tag{B10}$$

where we write

$$\delta f_{ia} = f_{ia} - \bar{f}_i \tag{B11}$$

and

$$\overline{f_i g_j} = \sum_{a=1}^{n} M_a f_{ia} g_{ja} \tag{B12}$$

Equation (B10) requires the tensor in parentheses to be symmetric, i.e.

$$e_{mjk}\beta_j\overline{\delta x_k x_n} - \overline{\delta v_m x_n} = e_{njk}\beta_j\overline{\delta x_k x_m} - \overline{\delta v_n x_m} \tag{B13}$$

which defines three independent equations in the unknowns $\boldsymbol{\beta}$. These equations may be written in the form

$$B_{ij}\beta_j = b_i \tag{B14}$$

where

$$B_{ij} = (\overline{\delta x_k x_k})\,\delta_{ij} - \overline{\delta x_i x_j} \tag{B15}$$

and

$$b_i = e_{ijk}\overline{\delta v_k x_j} \tag{B16}$$

From (B14) we have

$$\beta_j = B_{ji}^{-1} b_i \tag{B17}$$

Combining the above results we finally obtain

$$v_{ia}^{\mathrm{sli}} = P_{iakb} v_{kb} \tag{B18}$$

The projection matrix $\mathbf{P}$ has the structure

$$\mathbf{P} = \left(\mathbf{I} - \frac{\nabla g \otimes \nabla g}{|\nabla g|^2}\right)\tilde{\mathbf{P}} \tag{B19}$$

where

$$\tilde{P}_{iakb} = \delta_{ik}\delta_{ab} - \frac{M_b}{\bar{M}}\delta_{ik} - B_{jl}^{-1} M_b e_{jim} e_{lkn} \delta x_{ma} \delta x_{nb} \tag{B20}$$

ACKNOWLEDGEMENTS

CK, JEM and MO are grateful to the AFOSR for partial support through Caltech's MURI on Mathematical Infrastructure for Robust Virtual Engineering. MO is grateful to the DoE for partial support through Caltech's ASCI Center for the Simulation of the Dynamic Response of Materials. MO also wishes to gratefully acknowledge the support of the Army Research Office through grant DAAH04-96-1-0056. AP gratefully acknowledges helpful discussions with Dr Antonella Abbá of the Department of Mathematics of the Politecnico di Milano.

REFERENCES

1. Kane C, Repetto EA, Ortiz M, Marsden JE. Finite element analysis of nonsmooth contact. *Computer Methods in Applied Mechanics and Engineering* 1999; **180**:1–26.
2. Camacho GT, Ortiz M. Computational modelling of impact damage in brittle materials. *International Journal of Solids and Structures* 1996; **33**:2899–2938.
3. Ortiz M. Computational micromechanics. *Computational Mechanics* 1996; **18**:321–338.
4. Stein E, Wriggers P. Calculation of impact contact problems of thin elastic shells taking into account geometrical nonlinearities within the contact region. *Computer Methods in Applied Mechanics and Engineering* 1982; **34**:861–880.
5. Endo T, Oden JT, Becker Becke EB, Miller T. A numerical-analysis of contact and limit-point behavior in a class of problems of finite elastic-deformation. *Computers and Structures* 1984; **18**:899–910.
6. Bathe KJ, Chaudhary A. A solution method for planar and axisymmetric contact problems. *International Journal for Numerical Methods in Engineering* 1985; **21**:65–88.
7. Simo JC, Wriggers P, Taylor RL. A perturbed Lagrangian formulation for the finite-element solution of contact problems. *Computer Methods in Applied Mechanics and Engineering* 1985; **50**:163–180.
8. Wriggers P, Simo JC. A note on tangent stiffness for fully nonlinear contact problems. *Communications in Applied Numerical Methods* 1985; **1**:199–203.
9. Nouromid B, Wriggers P. A 2-level iteration method for solution of contact problems. *Computer Methods in Applied Mechanics and Engineering* 1986; **54**:131–144.
10. Oden JT, Lin TL. On the general rolling-contact problem for finite deformations of a viscoelastic cylinder. *Computer Methods in Applied Mechanics and Engineering* 1986; **57**:297–367.
11. Simo JC, Wriggers P, Schweizerhof KH, Taylor RL. Finite deformation post-buckling analysis involving inelasticity and contact constraints. *International Journal for Numerical Methods in Engineering* 1986; **23**: 779–800.
12. Bathe KJ, Mijailovich SS. Finite-element analysis of frictional contact problems. *Journal de Mecanique Theorique et Appliquee* 1988; **7**:31–45.
13. Bathe KJ. Some remarks and references on recent developments in finite-element analysis procedures. *Computers and Structures* 1991; **40**:201–202.
14. Carpenter NJ, Taylor RL, Katona MG. Lagrange constraints for transient finite-element surface-contact. *International Journal for Numerical Methods in Engineering* 1991; **32**:103–128.
15. Eterovic AL, Bathe KJ. On the treatment of inequality constraints arising from contact conditions in finite-element analysis. *Computers and Structures* 1991; **40**:203–209.
16. Papadopoulos P, Taylor RL. A mixed formulation for the finite-element solution of contact problems. *Computer Methods in Applied Mechanics and Engineering* 1992; **94**:373–389.
17. Zavarise G, Wriggers P, Stein E, Schrefler BA. A numerical-model for thermomechanical contact based on microscopic interface laws. *Mechanics Research Communications* 1992; **19**:173–182.
18. Zavarise G, Wriggers P, Stein E, Schrefler BA. Real contact mechanisms and finite-element formulation—a coupled thermomechanical approach. *International Journal for Numerical Methods in Engineering* 1992; **35**:767–785.
19. Papadopoulos P, Taylor RL. A simple algorithm for 3-dimensional finite-element analysis of contact problems. *Computers and Structures* 1993; **46**:1107–1118.
20. Taylor RL, Papadopoulos P. On a finite-element method for dynamic contact impact problems. *International Journal for Numerical Methods in Engineering* 1993; **36**:2123–2140.
21. Wriggers P, Zavarise G. Thermomechanical contact—a rigorous but simple numerical approach. *Computers and Structures* 1993; **46**:47–53.
22. Wriggers P, Imhof M. On the treatment of nonlinear unilateral contact problems. *Archive of Applied Mechanics Ingenieur Archiv* 1993; **63**:116–129.
23. Wriggers P, Zavarise G. Application of augmented Lagrangian techniques for nonlinear constitutive laws in contact interfaces. *Communications in Numerical Methods in Engineering* 1993; **9**:815–824.

24. Wriggers P, Miehe C. Contact constraints within coupled thermomechanical analysis—a finite-element model. *Computer Methods in Applied Mechanics and Engineering* 1994; **113**:301–319.
25. Wriggers P, Scherf O. An adaptive finite-element algorithm for contact problems in plasticity. *Computational Mechanics* 1995; **17**:88–97.
26. Bathe KJ, Bouzinov PA. On the constraint function-method for contact problems. *Computers and Structures* 1997; **64**:1069–1085.
27. Wriggers P, Zavarise G. On contact between 3-dimensional beams undergoing large deflections. *Communications in Numerical Methods in Engineering* 1997; **13**:429–438.
28. Pires EB, Oden JT. Analysis of contact problems with friction under oscillating loads. *Computer Methods in Applied Mechanics and Engineering* 1983; **39**:337–362.
29. Oden JT, Pires EB. Algorithms and numerical results for finite-element approximations of contact problems with non-classical friction laws. *Computers and Structures* 1984; **19**:137–147.
30. Chaudhary AB, Bathe KJ. A solution method for static and dynamic analysis of 3-dimensional contact problems with friction. *Computers and Structures* 1986; **24**:855–873.
31. Rabier PJ, Martins JAC, Oden TJ, Campos L. Existence and local uniqueness of solutions to contact problems in elasticity with nonlinear friction laws. *International Journal of Engineering Science* 1986; **24**:1755–1768.
32. Martins JAC, Oden JT. Existence and uniqueness results for dynamic contact problems with nonlinear normal and friction interface laws. *Nonlinear Analysis Theory Methods and Applications* 1987; **11**:407–428.
33. Rabier PJ, Oden JT. Solution to Signorini-like contact problems through interface models. 1. preliminaries and formulation of a variational equality. *Nonlinear Analysis Theory Methods and Applications* 1987; **11**: 1325–1350.
34. Ju JW, Taylor RL. A perturbed Lagrangian formulation for the finite-element solution of nonlinear frictional contact problems. *Journal de Mecanique Theorique et Appliquee* 1988; **7**:1–14.
35. Rabier PJ, Oden JT. Solution to Signorini-like contact problems through interface models. 2. existence and uniqueness theorems. *Nonlinear Analysis Theory Methods and Applications* 1988; **12**:1–17.
36. White L, Oden JT. Dynamics and control of viscoelastic solids with contact and friction effects. *Nonlinear Analysis Theory Methods and Applications* 1989; **13**:459–474.
37. Wriggers P, Van TV, Stein E. Finite-element formulation of large deformation impact-contact problems with friction. *Computers and Structures* 1990; **37**:319–331.
38. Peric D, Owen DRJ. Computational model for 3-d contact problems with friction based on the penalty method. *International Journal for Numerical Methods in Engineering* 1992; **35**:1289–1309.
39. Lee CY, Oden JT. A priori error estimation of hp-finite element approximations of frictional contact problems with normal compliance. *International Journal of Engineering Science* 1993; **31**:927–952.
40. Lee CY, Oden JT. Theory and approximation of quasi-static frictional contact problems. *Computer Methods in Applied Mechanics and Engineering* 1993; **106**:407–429.
41. Lee CY, Oden JT. A-posteriori error estimation of hp finite-element approximations of frictional contact problems. *Computer Methods in Applied Mechanics and Engineering* 1994; **113**:11–45.
42. Zavarise G, Wriggers P, Schrefler BA. On augmented Lagrangian algorithms for thermomechanical contact problems with friction. *International Journal for Numerical Methods in Engineering* 1995; **38**:2929–2949.
43. Neto EAD, Hashimoto K, Peric D, Owen DRJ. A phenomenological model for frictional contact accounting for wear effects. *Philosophical Transactions of the Royal Society of London* 1996; **A354**:819–843.
44. Cocu M. Existence of solutions of signorini problems with friction. *International Journal of Engineering Sciences* 1984; **22**:567–575.
45. Moreau JJ. Unilateral contact and dry friction in finite freedom dynamics. In *International Centre for Mechanical Sciences*, *Courses and Lectures*, Moreau JJ, Panagiotopoulos PD (eds). vol. 302. Springer: Vienna, 1988.
46. Klarbring A, Bjorkman G. A mathematical programming approach to contact problems with friction and varying contact surface. *Computers and Structures* 1988; **30**:1185–1198.
47. Jean M. Unilateral contact and dry friction: time and space variables discretization. *Archchiwum Mechaniki Warszawa* 1988; **40**:677–691.
48. Simo JC, Laursen TA. An augmented Lagrangian treatment of contact problems involving friction. *Computers and Structures* 1992; **42**:97–116.
49. Jean M. Frictional contact in rigid or deformable bodies: Numerical simulations of geomaterials. In *Mechanics of Geomaterial Interfaces*, Salvadurai APS, Boulon JM (eds). Elsevier Science: Amsterdam, 1995, 463–486.
50. Glocker C, Pfeiffer F. *Multibody Dynamics with Unilateral Contacts*. Wiley: New York, 1996.
51. Stromberg N. A newton method for three dimensional fretting problems. *European Journal of Mechanics A/Solids* 1997; **16**:573–593.
52. Christiansen PW, Klarbring A, Pang JS, Stromberg N. Formulation and comparison of algorithms for frictional contact problems. *International Journal for Numerical Methods in Engineering* 1998; **42**:145–173.
53. Anitescu M, Potra FA, Steward DE. Time-stepping for three-dimensional rigid body dynamics. *Computer Methods in Applied Mechanics and Engineering* 1999; **177**:183–197.

54. Glocker Ch. Formulation of spatial contact situations in rigid multibody systems. *Computer Methods in Applied Mechanics and Engineering* 1999; **177**:199–214.
55. Jean M. The nonsmooth contact dynamics method. *Computer Methods in Applied Mechanics and Engineering* 1999; **177**:235–257.
56. Laursen TA. On the development of thermodynamically consistent algorithms for thermomechanical frictional contact. *Computer Methods in Applied Mechanics and Engineering* 1999; **177**:273–287.
57. Pfeiffer F. Unilateral problems of dynamics. *Archive of Applied Mechanics* 1999; **69**:503–527.
58. Clarke FH. *Optimization and Nonsmooth Analysis*. Wiley: New York, 1983.
59. Panagiotopoulos PD. *Inequality Problems in Mechanics and Applications.* Birkhauser: Boston, 1985.
60. Kikuchi N, Oden JT. *Contact Problems in Elasticity*: *A Study of Variational Inequalities and Finite Element Methods*. SIAM: Philadelphia, PA, 1988.
61. Ortiz M. Topics in Constitutive Theory for Inelastic Solids. *PhD Thesis*, University of California at Berkeley, Berkeley: CA, 1981.
62. Ortiz M, Pinsky PM, Taylor RL. Operator split methods for the numerical solution of the elastoplastic dynamic problem. *Computer Methods in Applied Mechanics and Engineering* 1983; **39**:137–157.
63. Pinsky PM, Ortiz M, Taylor RL. Operator split methods for the numerical solution of the finite-deformation elastoplastic dynamic problem. *Computers and Structures* 1983; **17**:345–359.
64. Ortiz M, Stainier L. The variational formulation of viscoplastic constitutive updates. *Computer Methods in Applied Mechanics and Engineering* 1999; **171**:419–444.
65. Laursen TA, Govindjee S. A note on the treatment of frictionless contact between nonsmooth surfaces in fully nonlinear problems. *Communications in Numerical Methods in Engineering* 1994; **10**:869–878.
66. Radovitzky R, Ortiz M. Error estimation and adaptive meshing in strongly nonlinear dynamic problems. *Computer Methods in Applied Mechanics and Engineering* 1999; **172**:203–240.
67. Ortiz M, Repetto EA. Nonconvex energy minimization and dislocation structures in ductile single crystals. *Journal of the Mechanics and Physics of Solids* 1999; **47**(2):397–462.
68. Marsden JE, Ratiu TS. Texts in applied mathematics. In *Mechanics and Symmetry*, vol. 17. Springer Verlag: Berlin, 1994.
69. Belytschko T. An overview of semidiscretization and time integration procedures. In *Computational Methods for Transient Analysis*, Belytschko T, Hughes TJR (eds). North-Holland: Amsterdam, 1983; pages 1–65.
70. Hughes TJR. Analysis of transient algorithms with particular reference to stability behavior. In *Computational Methods for Transient Analysis*, Belytschko T, Hughes TJR (eds). North-Holland: Amsterdam, 1983; 67–155.
71. Spellucci P. A new technique for inconsistent QP problems in the SQP method. *Technical Report*, Technical University at Darmstadt, 1993.
72. Goldfarb D, Idnani A. A numerically stable dual method for solving strictly quadratic programs. *Mathematical Programming* 1983; **27**:1–33.
73. Boggs PT, Tolle JW. Sequential quadratic programming. *Acta Numerica* 1995; **4**:1–51.
74. Truesdell C. A simple example of an initial-value problem with any desired number of solutions. *Instituto Lombardo Accademia di Scienze Lettere Rendiconti* 1974; **A108**:301–304.
75. Kane C, Marsden JE, Ortiz M, West M. Variational integrators and the Newmark algorithm for conservative and dissipative mechanical systems. *International Journal for Numerical Methods in Engineering* 2000; **49**(10): 1295–1325.
76. Preparata FP, Shamos MI. *Computational Geometry*: *An Introduction*. Springer: New York, 1985.

